The testis-specific LINC component SUN3 is essential for sperm head shaping during mouse spermiogenesis

Received for publication, December 18, 2019, and in revised form, March 6, 2020 Published, Papers in Press, March 10, 2020, DOI 10.1074/jbc.RA119.012375

Qian Gao[‡1], Ranjha Khan[‡1], Changping Yu[‡], Manfred Alsheimer[§2], Xiaohua Jiang[‡3], Hui Ma[‡4], and Qinghua Shi[‡5]

From the [‡]First Affiliated Hospital of the University of Science and Technology of China, Hefei National Laboratory for Physical Sciences at Microscale, Chinese Academy of Sciences Key Laboratory of Innate Immunity and Chronic Diseases, School of Life Sciences, Chinese Academy of Sciences Center for Excellence in Molecular Cell Science, Collaborative Innovation Center of Genetics and Development, University of Science and Technology of China, Hefei 230027, China and the [§]Department of Cell and Developmental Biology, Biocenter, University of Würzburg, 97074 Würzburg, Germany

Edited by Qi-Qun Tang

Sperm head shaping is a key event in spermiogenesis and is tightly controlled via the acrosome–manchette network. Linker of nucleoskeleton and cytoskeleton (LINC) complexes consist of Sad1 and UNC84 domain–containing (SUN) and Klarsicht/ANC-1/Syne-1 homology (KASH) domain proteins and form conserved nuclear envelope bridges implicated in transducing mechanical forces from the manchette to sculpt sperm nuclei into a hook-like shape. However, the role of LINC complexes in sperm head shaping is still poorly understood. Here we assessed the role of SUN3, a testis-specific LINC component harboring a conserved SUN domain, in spermiogenesis. We show that CRISPR/Cas9-generated *Sun3* knockout male mice are infertile, displaying drastically reduced sperm counts and a globozoospermia-like phenotype, including a missing, mislocalized, or fragmented acrosome, as well as multiple defects in sperm flagella. Further examination revealed that the sperm head abnormalities are apparent at step 9 and that the sperm nuclei fail to elongate because of the absence of manchette microtubules and perinuclear rings. These observations indicate that *Sun3* deletion likely impairs the ability of the LINC complex to transduce the cytoskeletal force to the nuclear envelope, required for sperm head elongation. We also found that SUN3 interacts with SUN4 in mouse testes and that the level of SUN4 proteins is drastically reduced in *Sun3*-null mice. Altogether, our results indicate that SUN3 is essential for sperm head shaping and male fertility, providing molecular clues regarding the underlying pathology of the globozoospermia-like phenotype.

Spermiogenesis involves drastic morphological changes of spermatids, including acrosome formation, elongation and condensation of the nucleus, and disposal of residual cytoplasm, to differentiate into mature spermatozoa consisting of a head and a tail (1, 2). During this complex process, a transient cytoskeletal structure called the manchette appears concurrently with spermatid nucleus elongation. The manchette, which is first evident in step 8 spermatids in mice (3), is composed of parallel arrays of microtubules aligned with the long axis of the nucleus and a belt-like perinuclear ring made of actins where the microtubules are anchored, forming a sleeve-like structure that encircles the spermatid nucleus (4–6). It is believed that manchette microtubules emanate from perinuclear rings, as these microtubules appear from the post-acrosomal region in mouse and bovine spermatids (7). As spermatids differentiate, the microtubular structure and the perinuclear ring move caudally to the posterior pole of spermatid nucleus, sculpting the nucleus into a hook-like morphology.

The important role of the manchette in sperm head shaping has been demonstrated in several studies in which disruption of manchette-related proteins resulted in various forms of sperm head abnormalities and eventually impaired male fertility. For example, loss of functional HOOK1 causes ectopic positioning of the manchette microtubular structure within spermatids, resulting in abnormal sperm head morphologies, such as club-shaped and crescent forms (8). Similarly, disruption of RIMBP3, a HOOK1-interacting protein located in the manchette, also causes ectopic positioning of manchette and sperm head abnormalities similar to those of *Hook1* mutant mice (9). The microtubule plus-end-tracking protein CLIP-170 localizes prominently to the manchette rings during manchette formation, and male mice with knockout of *Clip-170* are subfertile because of defective sperm head shaping and abnormal elongation of the manchette tubules (2, 10). Despite the essential role of the manchette in spermiogenesis, how the microtubule manchette is assembled and regulated remains poorly understood.

Sad1/UNC84 (SUN)[6] homology proteins are a family of nuclear membrane proteins that share a conserved C terminus,

This work was supported by National Natural Science Foundation of China (NSFC) Grant 31890780, 31630050 (to Q. S.), and 31871514 (to X. J.); National Key Research and Developmental Program of China Grants 2018YFC1004700 (to X. J.) and 2016YFC1000600 (to Q. S.); and Strategic Priority Research Program of the Chinese Academy of Sciences Grant XDB19000000. The authors declare that they have no conflicts of interest with the contents of this article.

This article contains Figs. S1–S4.

[1] Both authors contributed equally to this work.

[2] Supported by German Research Foundation Grants Al 1090/4-1 and Al 1090/4-2 (to M. A.).

[3] To whom correspondence may be addressed. E-mail: biojxh@ustc.edu.cn.

[4] To whom correspondence may be addressed. E-mail: clsmh@ustc.edu.cn.

[5] To whom correspondence may be addressed. E-mail: qshi@ustc.edu.cn.

[6] The abbreviations used are: SUN, Sad1 and UNC84; KASH, Klarsicht/ANC-1/Syne-1 homology; LINC, linker of nucleoskeleton and cytoskeleton; PNA, peanut agglutinin; PAS, periodic acid-Schiff.

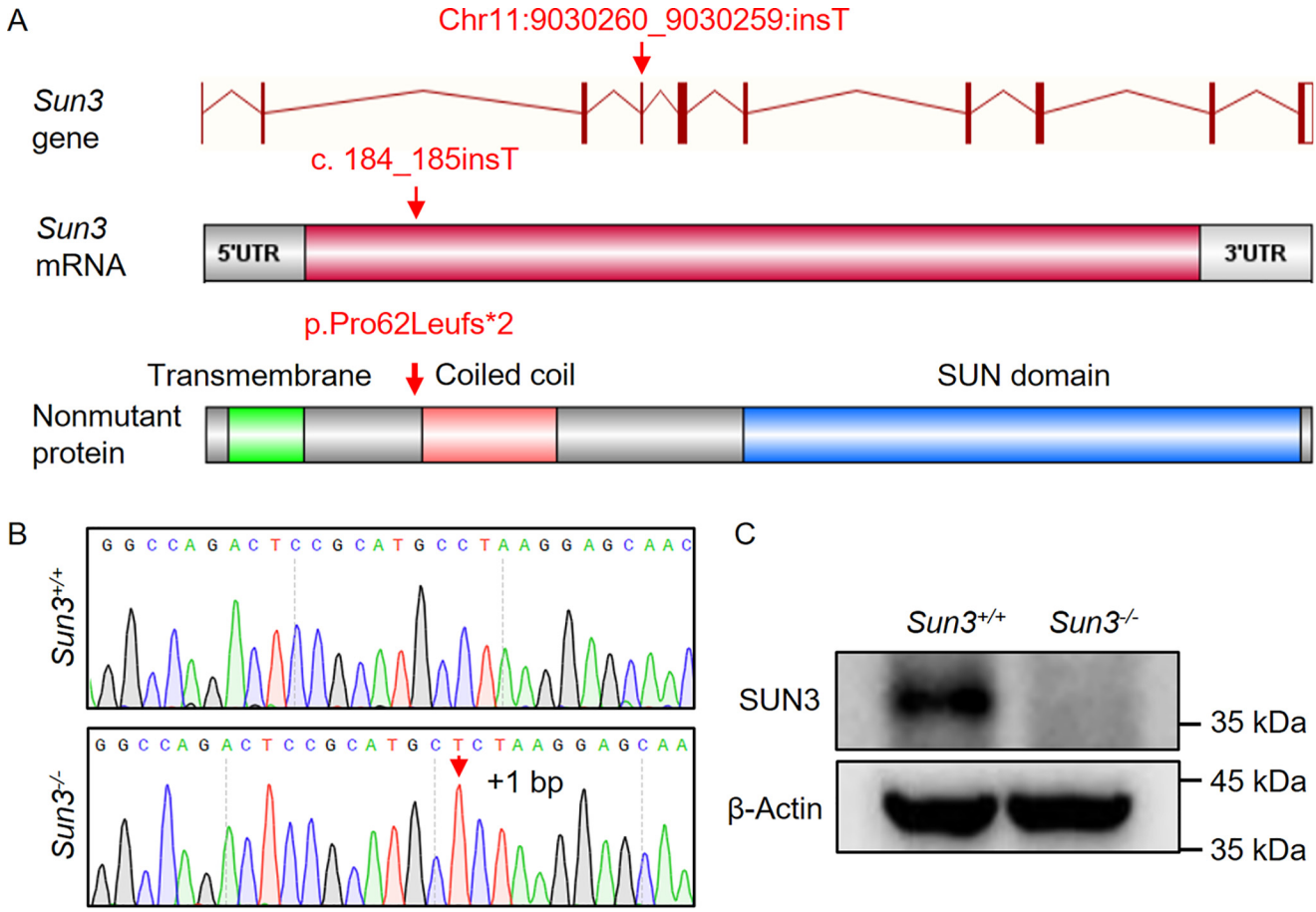

Figure 1. Generation of *Sun3*$^{-/-}$ mice. *A*, diagram illustrating the CRISPR/Cas9 targeting strategy to generate *Sun3* knockout mice. A thymine deoxyribotide was inserted in exon 4 between nucleotide positions 184 and 185, predicted to cause a frameshift at amino acid position 63 that introduces a premature stop codon at position 64 (p.Pro62Leufs*2). *B*, representative Sanger sequencing chromatograms showing the thymine deoxyribotide inserted between nucleotide positions 184 and 185, as indicated by the *red arrow*. *C*, Western blotting using the rabbit anti-SUN3 antibody confirms the lack of full-length SUN3 proteins in testis lysates from 8-week-old *Sun3*$^{-/-}$ mice.

the SUN domain. SUN proteins and Klarsicht/ANC-1/Syne-1 homology (KASH) proteins form a linker of nucleoskeleton and cytoskeleton (LINC) complex that functions like a bridge across the inner and outer nuclear membranes to physically connect the nucleus to the cytoskeleton (11). This complex is responsible for various important cellular functions, such as mechanotransduction, cellular signaling, nuclear anchorage, and positioning. So far, five SUN proteins have been described in mammals and have been demonstrated or suggested to play roles in germ cell development (12–17). SUN1 and SUN2 are ubiquitously expressed in various tissues (12, 13) and mediate meiotic telomere attachment to the nuclear envelope (18–22). SUN3, SUN4, and SUN5 are specifically expressed in the testes (14–17). SUN5 localization is restricted to the head–tail junctions of sperm and is essential for anchoring the sperm head to the tail (23). SUN4 localizes to the spermatid nuclear envelope in close association with manchette microtubules (15, 16). Knockout of *Sun4* in mice disrupts the lateral interactions of the manchette to the nucleus, and the nucleus thus fails to elongate, eventually resulting in a globozoospermia-like phenotype and male infertility (15, 16). SUN3 protein expression begins at postnatal day 15, and, similar to SUN4, its localization is closely associated with the manchette in developing spermatids (14). However, because of the lack of animal models, whether *Sun3* indeed plays a role in spermiogenesis is not clear.

To investigate the physiological functions of *Sun3* during mammalian spermatogenesis, we generated a *Sun3* knockout mouse model using CRISPR/Cas9 genome editing technology. We found that *Sun3*$^{-/-}$ male mice are infertile, displaying abnormal sperm head morphology and irregular acrosome localization, likely resulting from disruption of manchette assembly. These findings demonstrate that *Sun3* is essential for sperm head shaping during spermiogenesis.

Results

Generation of Sun3$^{-/-}$ *mice by CRISPR/Cas9-mediated genome editing*

Consistent with previous findings (14, 16), SUN3 was expressed testis-specifically (Fig. S1*A*) and was detected in spermatids, localizing to the nuclear pole distal to the acrosome and overlapping with α-tubulin and SUN4 (Fig. S1*B*). To investigate the biological function of SUN3, we generated *Sun3*-null mice using CRISPR/Cas9 genome editing technology (Fig. 1*A*). Sanger sequencing of genomic DNA from the mutant mice revealed that a thymidine was inserted between nucleotide position 184 and 185 (c.184_185insT) in exon 4 of *Sun3*, predicted to

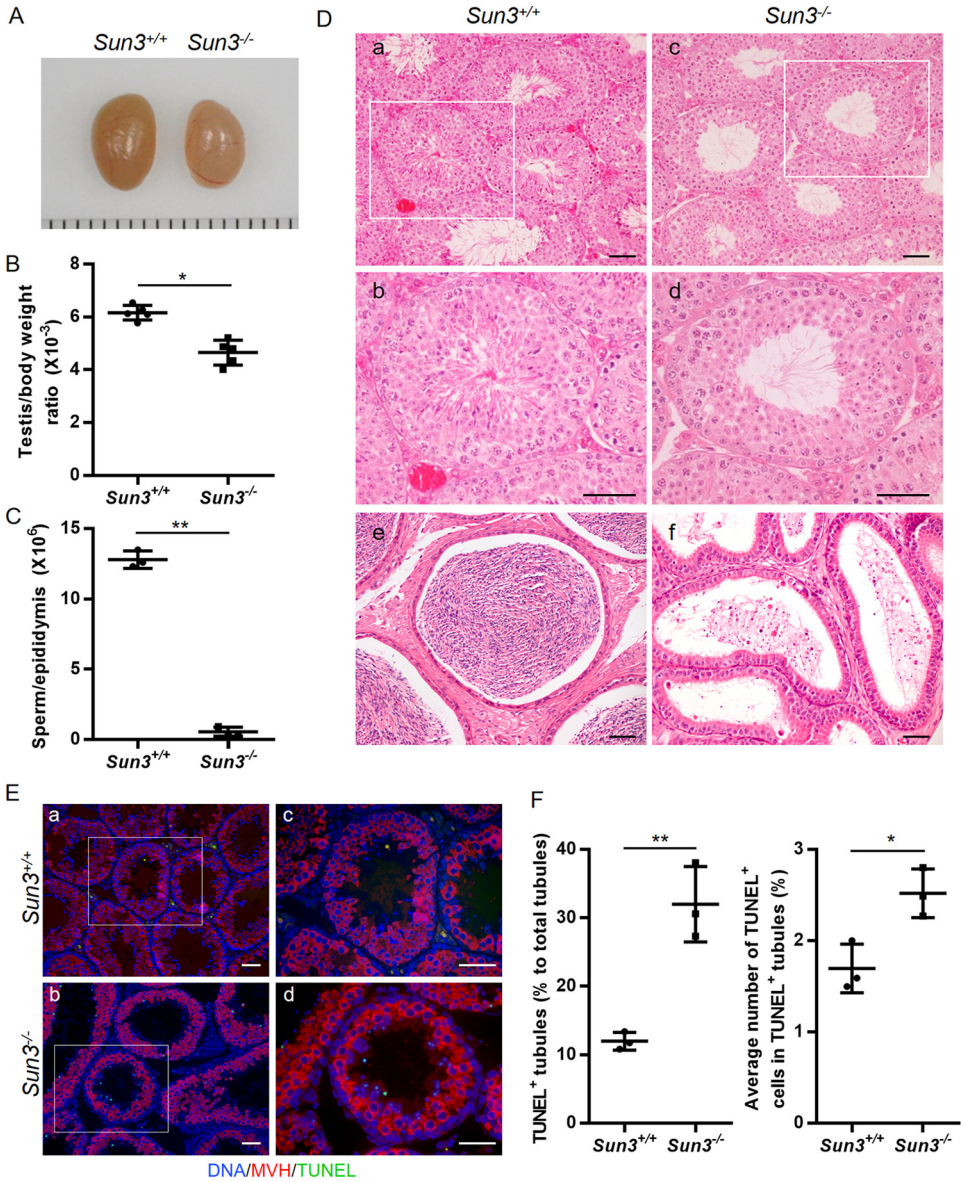

Figure 2. Deletion of *Sun3* impairs spermatogenesis. *A*, representative images of testes from 8-week-old *Sun3*$^{+/+}$ and *Sun3*$^{-/-}$ mice. Each grid represents 1 mm. *B*, average testes/body weight ratio of 8-week-old *Sun3*$^{+/+}$and *Sun3*$^{-/-}$ mice ($n = 5$). *C*, epididymal sperm number of 8-week-old *Sun3*$^{+/+}$ and *Sun3*$^{-/-}$ mice ($n = 3$). *D*, representative images of H&E-stained testicular sections (*a–d*) and epididymides (*e* and *f*) from 8-week-old *Sun3*$^{+/+}$ and *Sun3*$^{-/-}$ mice. *b* and *d*, higher-magnification images of the *rectangular area outlined with white boxes* in *a* and *c*, respectively. *Scale bars* = 50 μm. *E*, TUNEL assay performed on testicular sections from 8-week-old *Sun3*$^{+/+}$ and *Sun3*$^{-/-}$ mice. *c* and *d*, higher-magnification images of the *rectangular area outlined with white boxes* in *a* and *b*, respectively. *Scale bars* = 50 μm. *F*, percentage of TUNEL-positive tubules in testis sections from 8-week-old *Sun3*$^{+/+}$and *Sun3*$^{-/-}$ mice ($n = 3$). *F*, quantification of TUNEL-positive cells per TUNEL-positive tubule. 298 tubules were examined from three *Sun3*$^{+/+}$ mice. 375 tubules were examined from three *Sun3*$^{-/-}$ mice. Data are presented as mean ± S.D. Student's *t* test; *, $p < 0.05$; **, $p < 0.01$.

result in premature translation termination (p.Pro62Leufs*2) (Fig. 1*B*). Western blotting analyses further confirmed that full-length SUN3 proteins were absent in the testes of *Sun3*$^{-/-}$ mice (Fig. 1*C* and Fig. S2).

Deletion of Sun3 impairs spermatogenesis

Mice lacking *Sun3* appeared normal, displaying no obvious abnormalities in development and behavior. Given the testis-restricted expression pattern of SUN3, we studied fertility in *Sun3*$^{-/-}$ male mice. Mating attempts of *Sun3*$^{-/-}$ males with WT females did not produce any offspring, indicating that *Sun3*$^{-/-}$ males are infertile. *Sun3*$^{-/-}$ females showed no overt abnormalities in fertility.

Sun3$^{-/-}$ mice had smaller testes (Fig. 2, *A* and *B*) and sharply declined epididymal sperm numbers (0.17 ± 0.03 million/ml) compared with WT mice (12.80 ± 0.36 million/ml) (Fig. 2*C*). To further characterize the spermatogenic defects in *Sun3*$^{-/-}$ mice, H&E staining of testis and epididymis sections was performed. All types of spermatogenic cells were present in an orderly way in *Sun3*$^{+/+}$ seminiferous tubules and mature spermatozoa, and a canonical hook-shaped head could be seen in the lumen of tubules (Fig. 2*D*, *a* and *b*). However, in *Sun3*$^{-/-}$ mice, all elongating and elongated spermatids as well as spermatozoa were observed to have a noncanonical round head (Fig. 2*D*, *c* and *d*). Consistent with the result of sperm counting per epididymis, the numbers of these noncanonical spermatids

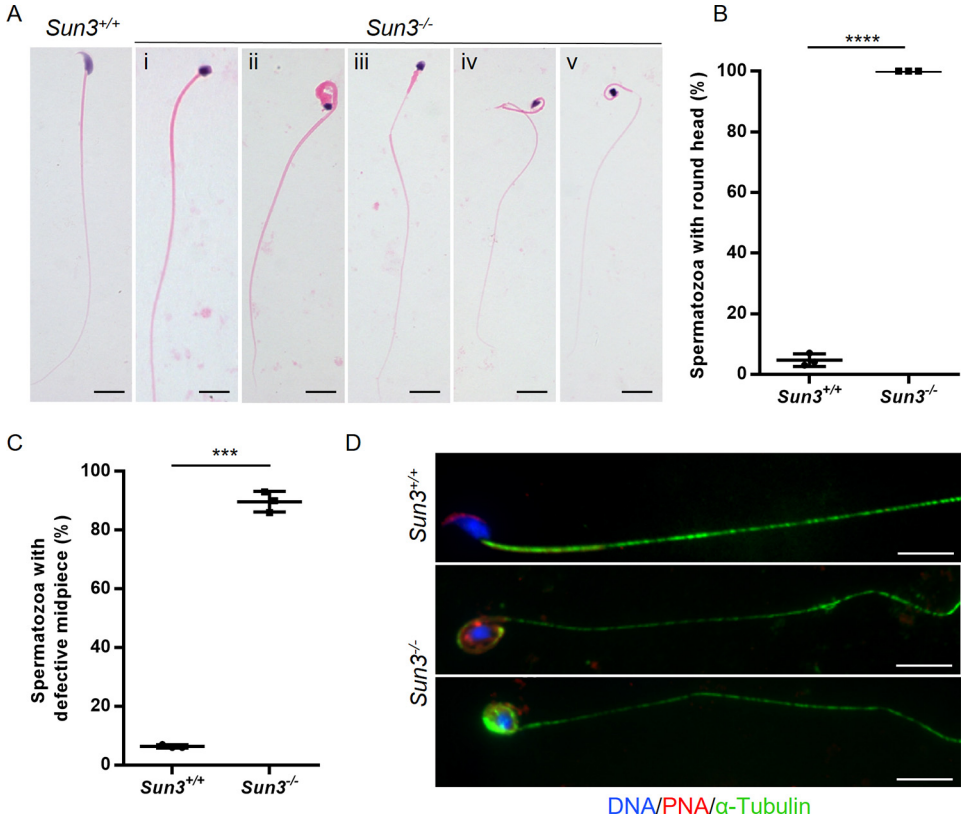

Figure 3. Morphological abnormalities of spermatozoa from *Sun3*$^{-/-}$ mice. *A*, representative images of spermatozoa from 8-week-old *Sun3*$^{+/+}$ and *Sun3*$^{-/-}$ mice. Spermatozoa from *Sun3*$^{+/+}$ mice present with typical morphology, whereas spermatozoa from *Sun3*$^{-/-}$ mice present an amorphous head accompanied by various midpiece defects, such as thickening (*i* and *ii*), coiling (*ii* and *v*), thinning (*iii*–*v*), and cracking (*iv*). *Scale bars* = 10 μm. *B*, quantification of spermatozoa with an amorphous head from 8-week-old *Sun3*$^{+/+}$ and *Sun3*$^{-/-}$ mice ($n = 3$). Student's *t* test; ****, $p < 0.0001$. *C*, quantification of spermatozoa with a defective midpiece from 8-week-old *Sun3*$^{+/+}$ and *Sun3*$^{-/-}$ mice ($n = 3$). Student's *t* test; ***, $p < 0.001$. *D*, representative images of spermatozoa from 8-week-old *Sun3*$^{+/+}$ and *Sun3*$^{-/-}$ mice stained for PNA (*red*) and α-tubulin (*green*). DNA was counterstained with Hoechst. *Scale bars* = 10 μm.

and spermatozoa were apparently lower in seminiferous tubules and in the cauda epididymides of *Sun3*$^{-/-}$ mice compared with those in *Sun3*$^{+/+}$ mice (Fig. 2*D*, *e* and *f*). Furthermore, a TUNEL assay in combination with a germ cell–specific marker (MVH) was performed, and the results indicated apoptosis in cells with a small amorphous nuclear shape, which corresponds to the noncanonical spermatids in *Sun3*$^{-/-}$ mice (Fig. 2*E*). The frequency of TUNEL^{+} tubules (11.99% ± 0.75% *versus* 32.00% ± 3.17%) and the number of TUNEL^{+} cells per TUNEL^{+} tubule (1.70% ± 0.15% *versus* 2.52% ± 0.15%) in *Sun3*$^{-/-}$ mice were significantly increased compared with *Sun3*$^{+/+}$ mice (Fig. 2*F*), suggesting that the spermatids of *Sun3*$^{-/-}$ mice underwent apoptosis. These results indicate that *Sun3* is essential for spermatogenesis and particularly for the development of spermatids.

Sun3$^{-/-}$ *mice produce round-headed spermatozoa*

We further analyzed the sperm morphology in the epididymis and found that, in contrast to the typical hook-shaped appearance of sperm heads in *Sun3*$^{+/+}$ mice, all sperm heads in *Sun3*$^{-/-}$ mice were amorphous with a smaller and more rounded shape (Fig. 3, *A* and *B*). Additionally, ~89.67% ± 2.02% of spermatozoa from *Sun3*$^{-/-}$ mice also displayed various midpiece defects, such as irregular caliber, bending, coiling, and/or cracking (Fig. 3, *A* and *C*, and Fig. S3). Immunofluorescence staining of peanut agglutinin (PNA), a marker of acrosomes, was performed on sperm smears and seminiferous tubules. In *Sun3*$^{+/+}$ mice, acrosomes with a typical crescent shape were found on top of the nucleus in the anterior dorsal part of the sperm head. However, acrosomes of spermatozoa from *Sun3*$^{-/-}$ mice were missing, mislocalized, or fragmented (Fig. 3*D*).

Because failure of sperm head elongation usually leads to a rounded head appearance, to understand the specific step at which head abnormalities occur in *Sun3*$^{-/-}$ mice, we compared spermatids of *Sun3*$^{+/+}$ and *Sun3*$^{-/-}$ mice at different steps of spermiogenesis. PAS staining revealed that the morphology of spermatids until steps 7 and 8 were comparable in *Sun3*$^{+/+}$ and *Sun3*$^{-/-}$ mice, indicating that the development of round spermatids was normal in *Sun3*$^{-/-}$ mice (Fig. 4). At step 9, the nuclei of spermatids became flattened and started to elongate along with condensation of chromatin in *Sun3*$^{+/+}$ mice, whereas in *Sun3*$^{-/-}$ mice, spermatids still had a round nucleus although the chromatin had been condensed. At step 10, spermatid nuclei in *Sun3*$^{+/+}$ mice became thinner and more elongated; however, the nuclei of spermatids were small and deformed and remained round in *Sun3*$^{-/-}$ mice (Fig. 4). We also noted that the number of spermatids was markedly reduced from step 10. Altogether, these findings demonstrate that abnormal morphology of *Sun3*$^{-/-}$ spermatids occurs when spermatids start to elongate.

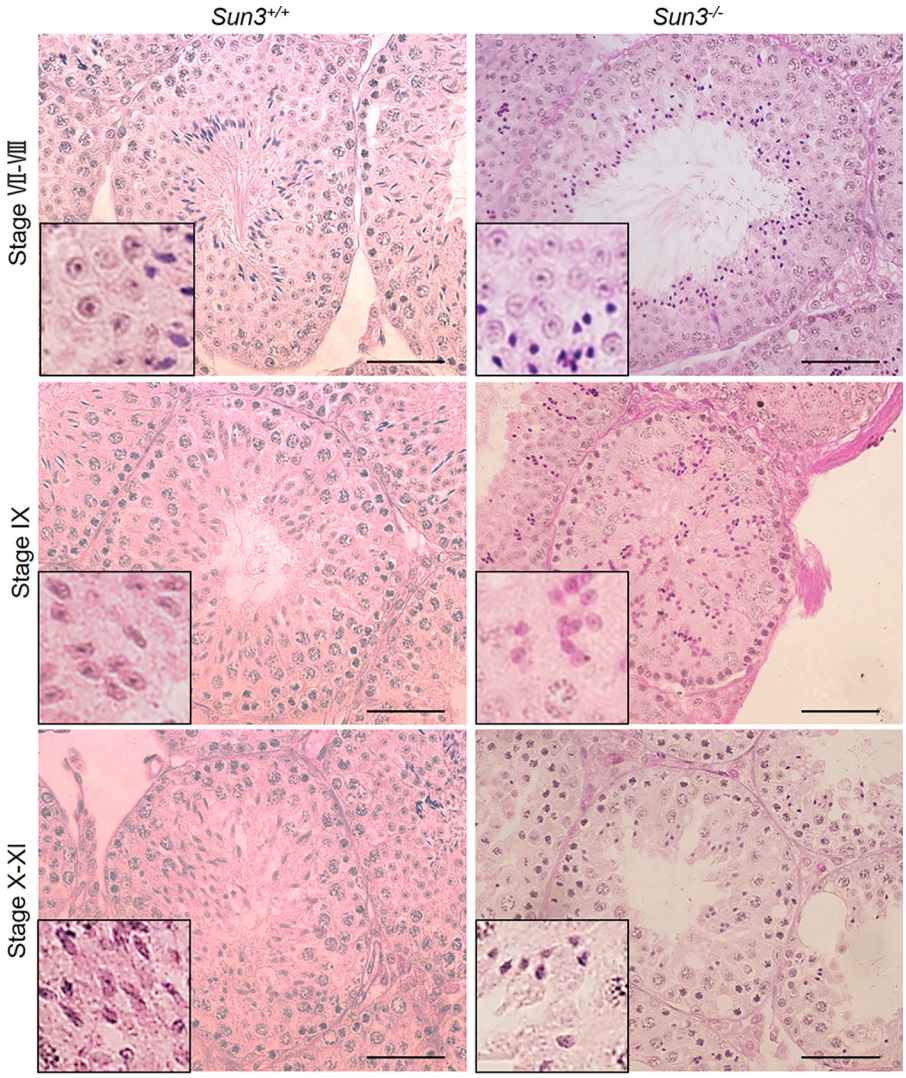

Figure 4. Abnormalities of spermatids occur when spermatids start to elongate in *Sun3*$^{-/-}$ mice. PAS staining of testis sections from 8-week-old *Sun3*$^{+/+}$ and *Sun3*$^{-/-}$ mice revealed abnormal sperm nuclei from step 9 in *Sun3*$^{-/-}$ mice. *Scale bars* = 50 μm.

Manchette assembly is disrupted in Sun3$^{-/-}$ *spermatids*

Because the microtubule manchette is essential for elongation of spermatids, and SUN3 localization is closely associated with the manchette (4, 14), we next wanted to find out whether the structure of the manchette was disrupted after *Sun3* deletion. Coimmunofluorescence staining of testis sections with antibodies against α-tubulin, a marker of manchette microtubules, and PNA was conducted. In *Sun3*$^{+/+}$ mice, manchette microtubules were found to be tightly attached to the nuclear periphery at the caudal region opposite the acrosome of spermatids; however, these structures were not detected in *Sun3*$^{-/-}$ mice despite some weak and diffuse labeling that was ectopically positioned (Fig. 5*A*). To confirm loss of manchette microtubules in *Sun3* knockout spermatids, immunofluorescence staining on testis cell smears was performed. In *Sun3*$^{+/+}$ mice, spermatids from step 1 to step 16 could be distinguished based on the morphology of the acrosome, and the acrosome covering the anterior side of the nucleus as well as the microtubules of the manchette tightly surrounding the caudal region could be seen from step 7/8 to step 14/15 in *Sun3*$^{+/+}$ spermatids. In *Sun3*$^{-/-}$ mice, we did not detect any morphological abnormalities in spermatids until step 7/8, and acrosomes covering the anterior side of the nucleus appeared to be normal in round spermatids. However, the typical microtubule arrays of the manchette were not observed in all spermatids from *Sun3*$^{-/-}$ mice. Aberrantly polymerized microtubule bundles that were dissociated from the nucleus were observed in about 5% of spermatids (Fig. 5*B*). Moreover, the perinuclear ring, a belt-like structure surrounding the nucleus where manchette microtubules insert, was also absent in spermatids from *Sun3*$^{-/-}$ mice (Fig. S4). Transmission EM (TEM) further revealed the presence of manchette microtubule bundles that were closely associated with the nuclear envelope in elongating spermatids from *Sun3*$^{+/+}$ testes; however, these recognizable structures were not seen in elongating spermatids from *Sun3*$^{-/-}$ testes, although some disorganized microtubule bundles that had lost their interaction with the nucleus were observed (Fig. 5*C*). Thus, we conclude that SUN3 is not only indispensable for manchette formation but also likely required for the organization of manchette during sperm head shaping in mice.

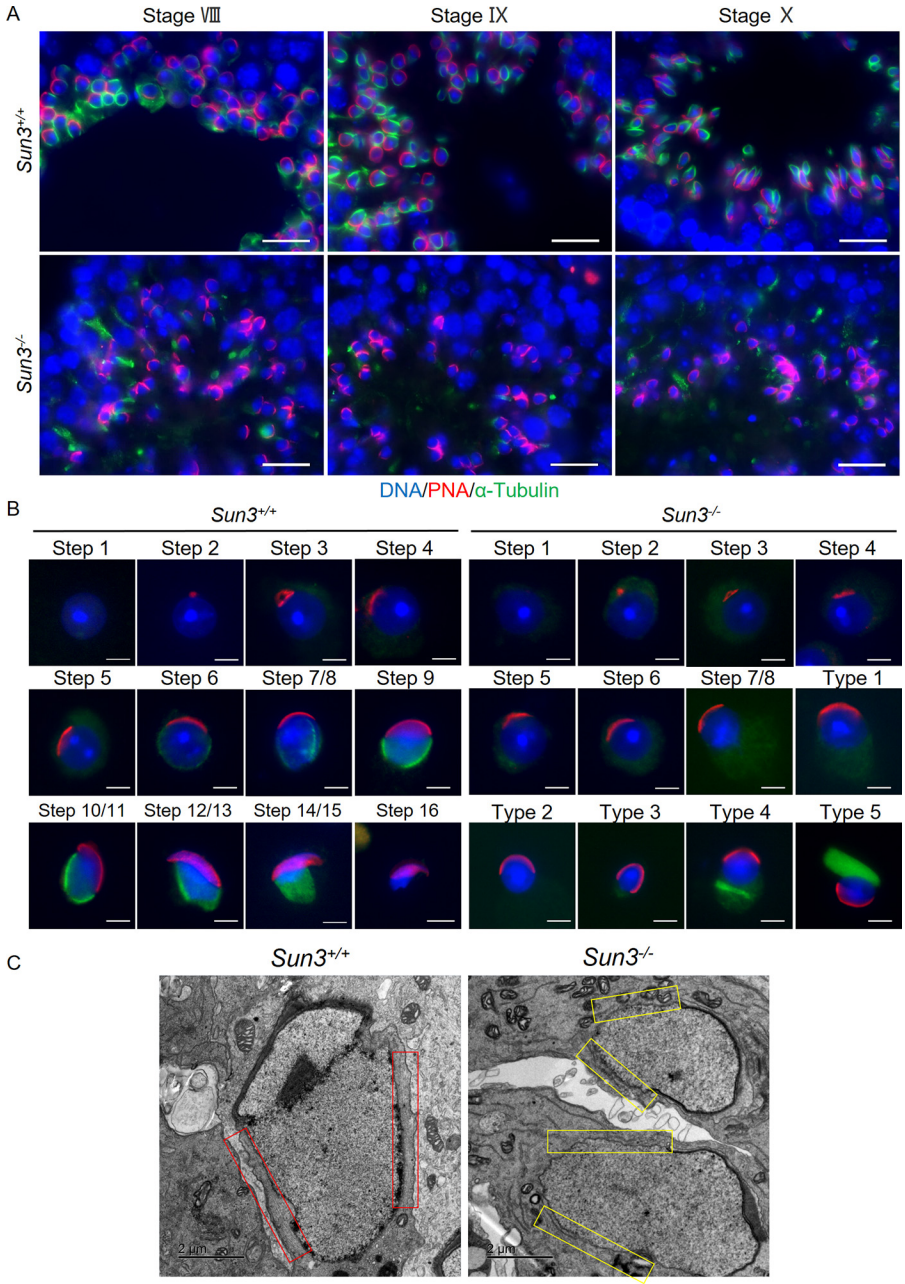

Figure 5. Manchette formation is disrupted in *Sun3*$^{-/-}$ mice. *A*, representative images of testis sections from 8-week-old *Sun3*$^{+/+}$ and *Sun3*$^{-/-}$ mice, stained by anti-PNA (*red*) and anti-α-tubulin (*green*) antibodies. DNA was counterstained with Hoechst. *Scale bars* = 20 μm. *B*, representative images of spermatids from 8-week-old *Sun3*$^{+/+}$ and *Sun3*$^{-/-}$ mice, stained by anti-PNA (*red*) and anti-α-tubulin (*green*) antibodies. DNA was counterstained with Hoechst. Types 1–5 show various abnormal spermatids in *Sun3*$^{-/-}$ mice. *Scale bars* = 2 μm. *C*, manchette microtubule bundles were not observed in Sun3$^{-/-}$ mice by transmission EM. *Red rectangles* show the presence of manchette microtubule bundles in *Sun3*$^{+/+}$ mice, whereas *yellow rectangles* indicate the absence of such microtubule bundles in *Sun3*$^{-/-}$ mice. *Scale bars* = 2 μm.

SUN3 interacts with SUN4 in mouse testes

Deletion of SUN4, another SUN protein that associates with the manchette, also leads to defects in acrosome and manchette formation in mice (15), similar to the findings in *Sun3*-null mice. To explore whether SUN3 interacts with SUN4 in testes, we performed immunoprecipitation using an anti-SUN3 antibody with testis lysates from *Sun3*$^{+/+}$ mice. Western blotting detected SUN3 and SUN4 in lysates immunoprecipitated by the anti-SUN3 antibody but not in IgG-immunoprecipitated lysates (Fig. 6, *A* and *B*). Immunofluorescence staining in *Sun3*$^{+/+}$ and *Sun3*$^{-/-}$ testicular sections revealed clear signals of SUN4 proteins surrounding the caudal region of the nucleus opposite the acrosome, where the manchette locates in step 7/8 spermatids, elongating spermatids, and elongated spermatids in *Sun3*$^{+/+}$ mice, whereas only unspecific diffuse signals were observed in the cytoplasm of spermatids from *Sun3*$^{-/-}$ mice (Fig. 6*C*). Western blotting of testicular lysates revealed that the level of SUN4 proteins was drastically reduced in adult *Sun3*$^{-/-}$ mice compared with *Sun3*$^{+/+}$ mice (Fig. 6*D*). These findings demonstrated that SUN3 and SUN4 interact and that SUN3 is required to maintain the level of SUN4 proteins *in vivo*.

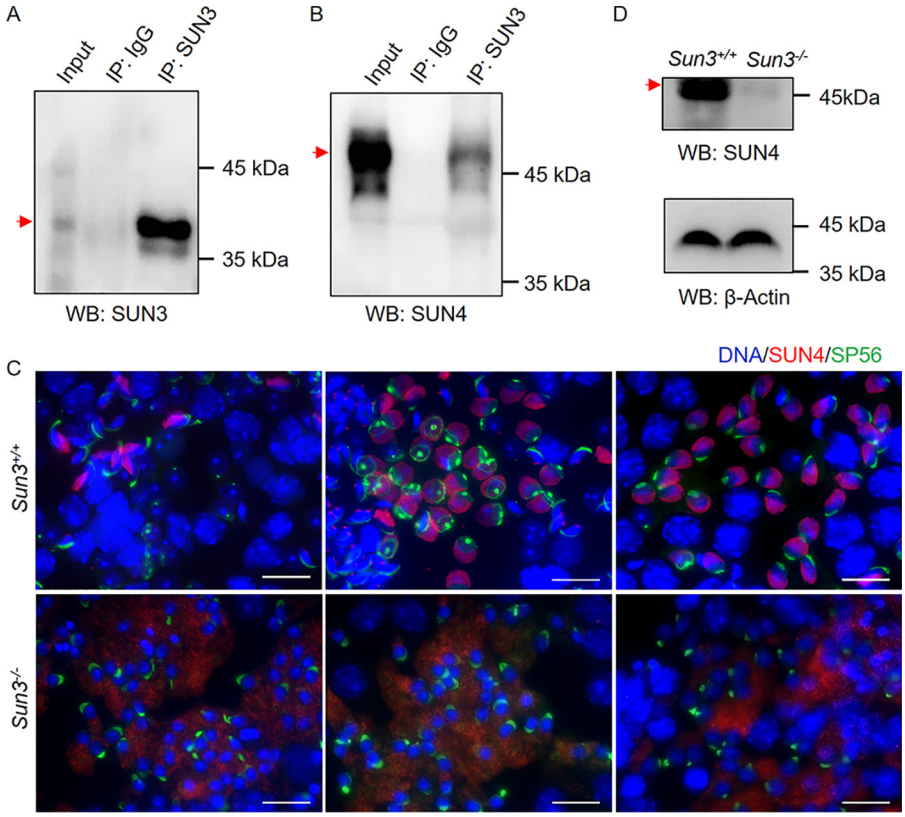

Figure 6. SUN3 interacts with SUN4 in mouse testes, and SUN4 protein levels are drastically reduced in *Sun3*$^{-/-}$ mice. *A*, Western blotting of immunoprecipitated testis extract showing the presence of SUN3 proteins in lysates immunoprecipitated by rabbit anti-SUN3 antibodies. Rabbit IgG was used as a negative control. *B*, Western blotting showing the presence of SUN4 proteins in testis lysates immunoprecipitated by guinea pig anti-SUN3 antibodies. Rabbit IgG was used as a negative control. *IP*, immunoprecipitation; *WB*, Western blotting. *C*, immunofluorescence staining of SUN4 (*red*), SP56 (*green*), and Hoechst (*blue*) on testis cell spreads from 8-week-old *Sun3*$^{+/+}$ and *Sun3*$^{-/-}$ mice, showing mislocalization of SUN4 in *Sun3*$^{-/-}$ spermatids. *Scale bars* = 20 μm. *D*, Western blotting showing the levels of SUN4 proteins in *Sun3*$^{+/+}$ and *Sun3*$^{-/-}$ testes. β-Actin was used as a loading control. For *A*, *B*, and *D*, the bands corresponding to the sizes of proteins of interest are indicated by *arrows*.

Discussion

Sperm head shaping is a key event during spermiogenesis, and misshaping of sperm heads often leads to male infertility (24). In this study, we generated mice lacking *Sun3* through CRISPR/Cas9 technology and investigated the function of SUN3 during spermiogenesis. We found that loss of SUN3 leads to a drastic reduction in sperm numbers, a globozoospermia-like phenotype accompanied by multiple sperm tail defects resulting from failure of manchette formation during sperm head shaping, and, ultimately, male infertility. Additionally, we also demonstrated that SUN3 interacts with SUN4 *in vivo* and is required to maintain the level of SUN4 proteins in testes. We report, for the first time, that *Sun3* is indispensable for sperm head shaping and particularly required for manchette formation.

A typical manchette is characterized by highly organized microtubule bundles attached to the perinuclear ring, forming a sleeve-like structure surrounding the posterior part of the spermatid nucleus (5, 25). This transient structure appears when spermatids are going to elongate and disappears when the sperm heads are properly shaped. Several genes have been reported to be implicated in manchette function in mice, including *Hook1*, *Katnb1*, *Lrguk1*, *Meig1*, *Pacrg*, and *Spef2* (8, 26–29). The manchettes in these mutant mice displayed a highly disorganized structure and/or perturbed disassembly, resulting in spermatozoa with a deformed shape (8, 26–29). However, we found that, in most cases, the canonical manchette structure was not detected in spermatids after *Sun3* knockout, and some aberrantly polymerized straight microtubule bundles were observed in a few step 8–16 spermatids (~5%), but these bundles were completely dissociated from the nucleus. The nuclear shape of the epididymal sperm from *Sun3* knockout mice was generally rounder than that observed in other disrupted manchettes. This suggests that SUN3 is essentially required for formation and coupling of the manchette.

SUN3 and SUN4 are exclusively expressed in spermatids and colocalize in close association with the manchette (14, 16, 30), suggesting a cooperative function in coupling of the manchette to the nuclear periphery so that the cytoplasmic forces can be transduced to shape the sperm nuclei. In *Sun4*$^{-/-}$ mice, manchette microtubules were disorganized, lost their lateral interaction with the nucleus, and, in some cases, were even completely missing, resulting in a globozoospermia-like phenotype (15). Deletion of *Sun4* caused SUN3 mislocalization with a tendency to form aggregates in the cytoplasm, suggesting that SUN3 localization depends on SUN4 (15). In this study, manchette tubules were not observed in the majority of spermatids in *Sun3*$^{-/-}$ mice, although a few spermatids showed some straight microtubule bundles, but these structures were disso-

ciated from nuclei, which closely resembled the phenotype of *Sun4*$^{-/-}$ mice. Interestingly, the level of SUN4 proteins was drastically reduced in *Sun3*$^{-/-}$ testes, indicating that SUN3 is also required to maintain the level of SUN4 proteins *in vivo*. Thus, it indicates that the functions of SUN3 and SUN4 are likely interdependent. It is worth mentioning that we tried many times to optimize the experimental protocols of coimmunoprecipitation using the anti-SUN4 antibody; however, we could not detect SUN3 in lysates immunoprecipitated by anti-SUN4 antibodies, for which the possibilities that anti-SUN4 antibody might not be suitable for coimmunoprecipitation experiments or that the interaction of SUN4 with the anti-SUN4 antibody may interfere with binding of SUN3 with SUN4 should be considered. It would be interesting to conduct further studies to confirm the interaction between SUN3 and SUN4, to investigate how SUN3 interacts with SUN4, and particularly how they coordinate and function in assembly or stabilization of the manchette cytoskeletal structure.

Anchorage and positioning of the cell nucleus plays an important role during diverse developmental processes such as fertilization, cell migration, and establishment of polarity (31–33). In mammalian somatic cells, the LINC complex, composed of SUN domain and KASH domain proteins, forms a protein bridge within the perinuclear space that connects the nucleus with the cytoskeleton (34, 35). Two spermiogenesis-specific LINC complexes have been described; one is SUN1η–NESPRIN3, localized on the anterior acrosomal side, and the other is SUN3–NESPRIN1, situated at the posterior pole of the spermatid nucleus (14). However, unlike the various functions of SUN proteins in spermatogenesis, the known KASH domain proteins appear to be not that important. Mice mutant for KASH domain proteins, *Nesprin1* or *Nesprin3*, were fully fertile, and disruption of genes encoding for other important KASH proteins (*Nesprin2*, *Nesprin4*, and *Lrmp*) also displayed no overt impact on fertility (36, 37). So far, only KASH5 has been shown to be essential for spermatogenesis. KASH5 is predominantly expressed at meiotic stages and aggregated at one nuclear pole in round and elongated spermatids (18). Mice lacking KASH5 manifested meiotic arrest; thus, we currently do not know whether KASH5 plays a role in spermiogenesis as well. However, given the localization pattern of KASH5 in spermatids, it is a poor candidate as a LINC complex partner for SUN3. Thus, we assume that NESPRIN1 is not essentially required for spermiogenesis and that SUN3 may form links with other alternative KASH proteins to physically couple the manchette to the nucleus.

Altogether, our study indicates that *Sun3* is required for sperm head shaping during mammalian spermiogenesis. Disruption of *Sun3* in mice caused a drastic reduction in sperm numbers and severe sperm head defects because of manchette formation failure, ultimately resulting in male infertility. These results will deepen our understanding of the role of LINC complexes in sperm head shaping and provide new molecular cues regarding the underlying pathology of globozoospermia.

Experimental procedures

Mice

Sun3$^{-/-}$ mice were generated using CRISPR/Cas9 genome editing as described previously (38). To generate *Sun3*$^{-/-}$ mice, a guide RNA sequence (GGCGTTGCTTAAAGACATGA) targeting exon 4 (5′-GACTCCGCATGCTCTAAGGA-3′) of the *Sun3* gene was coinjected with *Cas9* mRNAs into B6D2F1 (C57BL/6 × DBA/2) zygotes, which were subsequently transferred to the oviducts of pseudopregnant ICR female mice. Sanger sequencing of tail genomic DNA confirmed a female founder mouse carrying a homozygous 1-nt insertion in exon 4 of *Sun3* (5′-GACTCCGCATGCTCTAAGGA-3′, the inserted T nucleotide is underlined). The female founder mouse was crossed to WT C57BL/6 mice. The resulting heterozygous mice were crossed to obtain homozygous mutants. Animal experiments were approved by the Institutional Animal Care Committee of the University of Science and Technology of China. The following sequences of primers were used to confirm the genotype of *Sun3* mice: 5′-GGCAGGCTGAGAAAGACACACATG-3′ and 5′-GGCTTCACAGCTGACAATGGCAT-3′.

Western blotting

Testes from adult mice (8–12 weeks old) were homogenized in radioimmune precipitation assay buffer (25 mM Tris-HCl (pH 7.6), 150 mM NaCl, 1% NP-40, 1% sodium deoxycholate, and 0.1% SDS) supplemented with protease inhibitors using a Tissuelyzer and then cleared by centrifugation. Western blotting was carried out as described previously (39, 40). Antibodies included rabbit polyclonal anti-SUN3 (Proteintech, 26434-AP-1, 1:1000), guinea pig polyclonal anti-SUN3 (1:3000) (16), rabbit polyclonal anti-SUN4 (Proteintech, 19721-1-AP, 1:3000) and anti-β-actin (Abcam, ab8227, 1:100).

Sperm counting

Adult male mice were sacrificed by cervical dislocation. Their epididymides were dissected, minced into small pieces in 1 ml of Dulbecco's modified Eagle's medium, and incubated at 37 °C in a 5% CO_2 humidified incubator for 1 h to allow sperm release. Sperm counts were determined using a hemocytometer under a microscope (Nikon Eclipse E200).

Histological examination, TUNEL assay, and immunofluorescence staining

Mice were euthanized by cervical dislocation. Testes were removed and fixed overnight in Bouin's solution (for H&E and PAS) or 4% paraformaldehyde (for immunofluorescence staining and the TUNEL assay). Samples were dehydrated through a graded series of ethanol, embedded in paraffin, and sectioned at 5 μm for subsequent H&E and PAS staining. Sperm smears were prepared from epididymis as described previously (41). To prepare testis smears, testes were peeled off the testicular capsule, cut into pieces in PBS, and filtered through a 200-mesh cell strainer. The filtered cell suspensions were spread onto a glass slide.

H&E and PAS staining of tissue sections or sperm smears was performed as described previously (41). The TUNEL assay was

performed using the *In Situ* Cell Death Detection Kit (Roche, 11684795910) according to the manufacturer's instructions. For immunofluorescence, tissue sections, testis smears, or sperm smears were blocked in antibody dilution buffer (10% normal donkey serum, 3% BSA, and 0.05% Triton X-100 in PBS) for 30 min, followed by overnight incubation at 4 °C with primary antibodies against α-tubulin (Sigma, F2168, 1:200), rabbit polyclonal anti-SUN4 (1:3000), and lectin PNA (Invitrogen, L32458, 1:200). After washing with PBST four times, sections were incubated with secondary antibodies (Invitrogen, Alexa Fluor 488 goat anti-mouse IgG and Alexa Fluor 555 donkey anti-rabbit IgG, 1:200) at 37 °C for 1 h. Finally, sections were mounted with Vectashield mounting medium (Vector Laboratories, H-1000) containing Hoechst 33342 (Invitrogen, H21492). Staining of epididymal sperm mitochondria was performed using MitoTracker probes (Molecular Probes, M-7512). Images were captured using a Nikon Eclipse 80i microscope (Nikon) equipped with a digital camera incorporating a charge-coupled device (Hamamatsu) and analyzed using NIS-Element microscope imaging software (Nikon).

Coimmunoprecipitation

Tissue extracts were prepared using a Dounce homogenizer in cold immunoprecipitation buffer with 1% Triton X-100, 0.5% sodium deoxycholate, 0.1% SDS, 1 mM Na_3VO_4, 1 mM EDTA, 1 mM EGTA, 50 mM Tris (pH 7.5), and 150 mM NaCl dissolved in 500 ml of PBS supplemented with 1 mM phenylmethylsulfonyl fluoride and protein inhibitor mixture (Roche, 04693116001). All reagents were of analytical grade. Lysates were then centrifuged at 15,000 × *g* at 4 °C for 15 min, and the supernatant was divided into two aliquots. Each aliquot was incubated with 1.5 μg of rabbit anti-SUN3 antibody (Proteintech, 26434-AP-1) or rabbit IgG nonspecific antibody (CST, 2729S). After incubation at 4 °C overnight with rotation, beads were washed five times with radioimmune precipitation assay buffer. Finally, the beads were resuspended in 3× SDS-sample buffer (120 mM Tris/HCl, 10% SDS, 20% glycerol, 20% 2-mercaptoethanol, and bromphenol blue (pH 6.8)), boiled at 100 °C for 15 min, and subsequently subjected to Western blotting.

Transmission EM

Ultrastructural analysis of *Sun3*$^{-/-}$ mouse testes was performed as described previously (42). Briefly, testes from *Sun3*$^{+/+}$ and *Sun3*$^{-/-}$ mice were fixed in 4% paraformaldehyde containing 0.05% glutaraldehyde in 0.1 M phosphate buffer and then post-fixed in 1% osmium tetroxide. Dehydration was carried out in ethanol, and the samples were embedded in Epon 812. Ultrathin sections were obtained, counterstained with uranyl acetate and lead citrate, and examined with a JEOL JEM-1230 transmission electron microscope.

Statistical analysis

Testis/body weight ratio, sperm number, sperm morphology, and TUNEL-positive cells in *Sun3*$^{+/+}$ and *Sun3*$^{-/-}$ mice were analyzed statistically by using Student's *t* test. Results are presented as mean ± S.D. Statistical significance is defined as $p < 0.05$.

Author contributions—Q. G. and R. K. methodology; Q. G. and R. K. writing-original draft; C. Y. and M. A. resources; C. Y. visualization; M. A., X. J., H. M., and Q. S. writing-review and editing; X. J. and Q. S. conceptualization; H. M. formal analysis; Q. S. funding acquisition.

References

1. Jan, S. Z., Hamer, G., Repping, S., de Rooij, D. G., van Pelt, A. M., and Vormer, T. (2012) Molecular control of rodent spermatogenesis. *Biochim. Biophys. Acta* **1822,** 1838–1850 CrossRef Medline
2. Lehti, M. S., and Sironen, A. (2016) Formation and function of the manchette and flagellum during spermatogenesis. *Reproduction* **151,** R43-R54 CrossRef Medline
3. O'Donnell, L., and O'Bryan, M. K. (2014) Microtubules and spermatogenesis. *Semin. Cell Dev. Biol.* **30,** 45–54 CrossRef Medline
4. Kierszenbaum, A. L. (2001) Spermatid manchette: plugging proteins to zero into the sperm tail. *Mol. Reprod. Dev.* **59,** 347–349 CrossRef Medline
5. Courtens, J. L., and Loir, M. (1981) The spermatid manchette of mammals: formation and relations with the nuclear envelope and the chromatin. *Reprod. Nutr. Dev.* **21,** 467–477 CrossRef Medline
6. Kierszenbaum, A. L., and Tres, L. L. (2004) The acrosome-acroplaxome-manchette complex and the shaping of the spermatid head. *Arch. Histol. Cytol.* **67,** 271–284 CrossRef Medline
7. Moreno, R. D., and Schatten, G. (2000) Microtubule configurations and post-translational α-tubulin modifications during mammalian spermatogenesis. *Cell Motil. Cytoskeleton* **46,** 235–246 CrossRef Medline
8. Mendoza-Lujambio, I., Burfeind, P., Dixkens, C., Meinhardt, A., Hoyer-Fender, S., Engel, W., and Neesen, J. (2002) The Hook1 gene is non-functional in the abnormal spermatozoon head shape (azh) mutant mouse. *Hum. Mol. Genet.* **11,** 1647–1658 CrossRef Medline
9. Zhou, J., Du, Y.-R., Qin, W.-H., Hu, Y.-G., Huang, Y.-N., Bao, L., Han, D., Mansouri, A., and Xu, G.-L. (2009) RIM-BP3 is a manchette-associated protein essential for spermiogenesis. *Development* **136,** 373–382 CrossRef Medline
10. Akhmanova, A., Mausset-Bonnefont, A. L., van Cappellen, W., Keijzer, N., Hoogenraad, C. C., Stepanova, T., Drabek, K., van der Wees, J., Mommaas, M., Onderwater, J., van der Meulen, H., Tanenbaum, M. E., Medema, R. H., Hoogerbrugge, J., Vreeburg, J., *et al.* (2005) The microtubule plus-end-tracking protein CLIP-170 associates with the spermatid manchette and is essential for spermatogenesis. *Gene Dev.* **19,** 2501–2515 CrossRef Medline
11. Tzur, Y. B., Wilson, K. L., and Gruenbaum, Y. (2006) SUN-domain proteins: "velcro" that links the nucleoskeleton to the cytoskeleton. *Nat. Rev. Mol. Cell Biol.* **7,** 782–788 CrossRef Medline
12. Hodzic, D. M., Yeater, D. B., Bengtsson, L., Otto, H., and Stahl, P. D. (2004) Sun2 is a novel mammalian inner nuclear membrane protein. *J. Biol. Chem.* **279,** 25805–25812 CrossRef Medline
13. Padmakumar, V. C., Libotte, T., Lu, W., Zaim, H., Abraham, S., Noegel, A. A., Gotzmann, J., Foisner, R., and Karakesisoglou, I. (2005) The inner nuclear membrane protein Sun1 mediates the anchorage of Nesprin-2 to the nuclear envelope. *J. Cell Sci.* **118,** 3419–3430 CrossRef Medline
14. Göb, E., Schmitt, J., Benavente, R., and Alsheimer, M. (2010) Mammalian sperm head formation involves different polarization of two novel LINC complexes. *PLoS ONE* **5,** e12072 CrossRef Medline
15. Calvi, A., Wong, A. S., Wright, G., Wong, E. S., Loo, T. H., Stewart, C. L., and Burke, B. (2015) SUN4 is essential for nuclear remodeling during mammalian spermiogenesis. *Dev. Biol.* **407,** 321–330 CrossRef Medline
16. Pasch, E., Link, J., Beck, C., Scheuerle, S., and Alsheimer, M. (2015) The LINC complex component Sun4 plays a crucial role in sperm head formation and fertility. *Biol. Open* **4,** 1792–1802 CrossRef Medline
17. Yassine, S., Escoffier, J., Abi Nahed, R., Pierre, V., Karaouzene, T., Ray, P. F., and Arnoult, C. (2015) Dynamics of Sun5 localization during spermatogenesis in wild type and Dpy19l2 knock-out mice indicates that Sun5 is not involved in acrosome attachment to the nuclear envelope. *PLoS ONE* **10,** e0118698 CrossRef Medline

18. Morimoto, A., Shibuya, H., Zhu, X., Kim, J., Ishiguro, K., Han, M., and Watanabe, Y. (2012) A conserved KASH domain protein associates with telomeres, SUN1, and dynactin during mammalian meiosis. *J. Cell Biol.* **198,** 165–172 CrossRef Medline
19. Ding, X., Xu, R., Yu, J., Xu, T., Zhuang, Y., and Han, M. (2007) SUN1 is required for telomere attachment to nuclear envelope and gametogenesis in mice. *Dev. Cell* **12,** 863–872 CrossRef Medline
20. Penkner, A. M., Fridkin, A., Gloggnitzer, J., Baudrimont, A., Machacek, T., Woglar, A., Csaszar, E., Pasierbek, P., Ammerer, G., Gruenbaum, Y., and Jantsch, V. (2009) Meiotic Chromosome homology search involves modifications of the nuclear envelope protein Matefin/SUN-1. *Cell* **139,** 920–933 CrossRef Medline
21. Lei, K., Zhang, X., Ding, X., Guo, X., Chen, M., Zhu, B., Xu, T., Zhuang, Y., Xu, R., and Han, M. (2009) SUN1 and SUN2 play critical but partially redundant roles in anchoring nuclei in skeletal muscle cells in mice. *Proc. Natl. Acad. Sci. U.S.A.* **106,** 10207–10212 CrossRef Medline
22. Link, J., Leubner, M., Schmitt, J., Göb, E., Benavente, R., Jeang, K.-T., Xu, R., and Alsheimer, M. (2014) Analysis of meiosis in SUN1 deficient mice reveals a distinct role of SUN2 in mammalian meiotic LINC complex formation and function. *PLoS Genet.* **10,** e1004099 CrossRef Medline
23. Shang, Y., Zhu, F., Wang, L., Ouyang, Y. C., Dong, M. Z., Liu, C., Zhao, H., Cui, X., Ma, D., Zhang, Z., Yang, X., Guo, Y., Liu, F., Yuan, L., Gao, F., *et al.* (2017) Essential role for SUN5 in anchoring sperm head to the tail. *Elife* **6,** e28199 CrossRef Medline
24. Yan, W. (2009) Male infertility caused by spermiogenic defects: lessons from gene knockouts. *Mol. Cell Endocrinol.* **306,** 24–32 CrossRef Medline
25. Kierszenbaum, A. L., Rivkin, E., and Tres, L. L. (2011) Cytoskeletal track selection during cargo transport in spermatids is relevant to male fertility. *Spermatogenesis* **1,** 221–230 CrossRef Medline
26. Dunleavy, J. E. M., Okuda, H., O'Connor, A. E., Merriner, D. J., O'Donnell, L., Jamsai, D., Bergmann, M., and O'Bryan, M. K. (2017) Katanin-like 2 (KATNAL2) functions in multiple aspects of haploid male germ cell development in the mouse. *PLoS Genet.* **13,** e1007078 CrossRef Medline
27. Liu, Y., DeBoer, K., de Kretser, D. M., O'Donnell, L., O'Connor, A. E., Merriner, D. J., Okuda, H., Whittle, B., Jans, D. A., Efthymiadis, A., McLachlan, R. I., Ormandy, C. J., Goodnow, C. C., Jamsai, D., and O'Bryan, M. K. (2015) LRGUK-1 is required for basal body and manchette function during spermatogenesis and male fertility. *PLoS Genet.* **11,** e1005090 CrossRef Medline
28. Lehti, M. S., Zhang, F.-P., Kotaja, N., and Sironen, A. (2017) SPEF2 functions in microtubule-mediated transport in elongating spermatids to ensure proper male germ cell differentiation. *Development* **144,** 2683–2693 CrossRef Medline
29. Li, W., Tang, W., Teves, M. E., Zhang, Z., Zhang, L., Li, H., Archer, K. J., Peterson, D. L., Williams, D. C., Jr., Strauss, J. F., 3rd, and Zhang, Z. (2015) A MEIG1/PACRG complex in the manchette is essential for building the sperm flagella. *Development* **142,** 921–930 CrossRef Medline
30. Shao, X., Tarnasky, H. A., Lee, J. P., Oko, R., and van der Hoorn, F. A. (1999) Spag4, a novel sperm protein, binds outer dense-fiber protein Odf1 and localizes to microtubules of manchette and axoneme. *Dev. Biol.* **211,** 109–123 CrossRef Medline
31. Fridkin, A., Penkner, A., Jantsch, V., and Gruenbaum, Y. (2009) SUN-domain and KASH-domain proteins during development, meiosis and disease. *Cell Mol. Life Sci.* **66,** 1518–1533 CrossRef Medline
32. Starr, D. A. (2009) A nuclear-envelope bridge positions nuclei and moves chromosomes. *J. Cell Sci.* **122,** 577–586 CrossRef Medline
33. Burke, B., and Roux, K. J. (2009) Nuclei take a position: managing nuclear location. *Dev. Cell* **17,** 587–597 CrossRef Medline
34. Sosa, B. A., Rothballer, A., Kutay, U., and Schwartz, T. U. (2012) LINC complexes form by binding of three KASH peptides to domain interfaces of trimeric SUN proteins. *Cell* **149,** 1035–1047 CrossRef Medline
35. Wang, W., Shi, Z., Jiao, S., Chen, C., Wang, H., Liu, G., Wang, Q., Zhao, Y., Greene, M. I., and Zhou, Z. (2012) Structural insights into SUN-KASH complexes across the nuclear envelope. *Cell Res.* **22,** 1440–1452 CrossRef Medline
36. Horn, H. F., Kim, D. I., Wright, G. D., Wong, E. S., Stewart, C. L., Burke, B., and Roux, K. J. (2013) A mammalian KASH domain protein coupling meiotic chromosomes to the cytoskeleton. *J. Cell Biol.* **202,** 1023–1039 CrossRef Medline
37. Zhang, X., Xu, R., Zhu, B., Yang, X., Ding, X., Duan, S., Xu, T., Zhuang, Y., and Han, M. (2007) Syne-1 and Syne-2 play crucial roles in myonuclear anchorage and motor neuron innervation. *Development* **134,** 901–908 CrossRef Medline
38. Jiang, L., Li, T., Zhang, X., Zhang, B., Yu, C., Li, Y., Fan, S., Jiang, X., Khan, T., Hao, Q., Xu, P., Nadano, D., Huleihel, M., Lunenfeld, E., Wang, P. J., *et al.* (2017) RPL10L is required for male meiotic division by compensating for RPL10 during meiotic sex chromosome inactivation in mice. *Curr. Biol.* **27,** 1498–1505.e6 CrossRef Medline
39. Jiang, X., Ma, T., Zhang, Y., Zhang, H., Yin, S., Zheng, W., Wang, L., Wang, Z., Khan, M., Sheikh, S. W., Bukhari, I., Iqbal, F., Cooke, H. J., and Shi, Q. (2015) Specific deletion of Cdh2 in Sertoli cells leads to altered meiotic progression and subfertility of mice. *Biol. Reprod.* **92,** 79 Medline
40. Yin, H., Ma, H., Hussain, S., Zhang, H., Xie, X., Jiang, L., Jiang, X., Iqbal, F., Bukhari, I., Jiang, H., Ali, A., Zhong, L., Li, T., Fan, S., Zhang, B., *et al.* (2019) A homozygous FANCM frameshift pathogenic variant causes male infertility. *Genet. Med.* **21,** 62 CrossRef Medline
41. Zhu, F., Yan, P., Zhang, J., Cui, Y., Zheng, M., Cheng, Y., Guo, Y., Yang, X., Guo, X., and Zhu, H. (2019) Deficiency of TPPP2, a factor linked to oligoasthenozoospermia, causes subfertility in male mice. *J. Cell. Mol. Med.* **23,** 2583–2594 CrossRef Medline
42. Zhang, B., Ma, H., Khan, T., Li, T., Zhang, H., Gao, J., Zhou, J., Ma, A., Li, Y., Yu, C., Bao, J., Ali, A., Murtaza, G., Yin, H., Gao, Q., *et al.* (2020) A DNAH17 missense variant causes flagella destabilization and asthenozoospermia. *J. Exp. Med.* **217,** e20182365 CrossRef Medline